

MM-ISTS: Cooperating Irregularly Sampled Time Series Forecasting with Multimodal Vision-Text LLMs

Zhi Lei*

zhilei@stu.ecnu.edu.cn
East China Normal University
Shanghai, China

Chenxi Liu*

chenxi.liu@cair-cas.org.hk
Centre for Artificial Intelligence and
Robotics, Hong Kong Institute of
Science & Innovation, Chinese
Academy of Sciences
Hong Kong, China

Hao Miao

haom@cs.aau.dk
Department of Computing, The Hong
Kong Polytechnic University
Hong Kong, China

Wanghui Qiu

onehui@stu.ecnu.edu.cn
East China Normal University
Shanghai, China

Bin Yang

byang@dase.ecnu.edu.cn
East China Normal University
Shanghai, China

Chenjuan Guo[†]

cjguo@dase.ecnu.edu.cn
East China Normal University
Shanghai, China

Abstract

Irregularly sampled time series (ISTS) are widespread in real-world scenarios, exhibiting asynchronous observations on uneven time intervals across variables. Existing ISTS forecasting methods often solely utilize historical observations to predict future ones while falling short in learning contextual semantics and fine-grained temporal patterns. To address these problems, we achieve MM-ISTS, a multimodal framework augmented by vision-text large language models, that bridges temporal, visual, and textual modalities, facilitating ISTS forecasting. MM-ISTS encompasses a novel two-stage encoding mechanism. In particular, a cross-modal vision-text encoding module is proposed to automatically generate informative visual images and textual data, enabling the capture of intricate temporal patterns and comprehensive contextual understanding, in collaboration with multimodal LLMs (MLLMs). In parallel, ISTS encoding extracts complementary yet enriched temporal features from historical ISTS observations, including multi-view embedding fusion and a temporal-variable encoder. Further, we propose an adaptive query-based feature extractor to compress the learned tokens of MLLMs, filtering out small-scale useful knowledge, which in turn reduces computational costs. In addition, a multimodal alignment module with modality-aware gating is designed to alleviate the modality gap across ISTS, images, and text. Extensive experiments on real data offer insight into the effectiveness of the proposed solutions.

Keywords

ISTS Forecasting, Multimodal LLMs, Cross-Modal Alignment

1 Introduction

The expanding instrumentation of processes throughout society with sensors yields a proliferation of time series data in various domains such as healthcare [8, 23], transportation [7, 29], climate science [2, 24], and astronomy [25, 32]. Existing time series forecasting methods [15, 21, 34] mainly focus on fully observed data and cannot adapt to irregularly sampled time series (ISTS) [18, 20, 41, 42], which

are more common in real-world scenarios due to sensor malfunctions, network failure, and varying sampling sources. ISTS exhibits asynchronous observations on non-uniform time intervals across variables [26], making it difficult to achieve accurate forecasting for potential informed decision-making [13].

Existing ISTS forecasting methods can be generally categorized into three paradigms based on how to model temporal irregularities. The first category focuses on continuous-time modeling [22, 44], which often utilizes differential equations or state-space models to naturally handle uneven time gaps. The second category methods employ geometric deep learning [13, 37] or patch-based modeling [18, 42] to capture dependencies among asynchronous observations via graph connectivity or segmented temporal tokens, which often involve aggregation or pooling operations that may obscure fine-grained temporal patterns. Recently, another line of methods has emerged that applies pre-trained language models (PLMs) [41] for ISTS forecasting due to the generalization capabilities of PLMs.

Despite these advancements, most existing methods remain confined to a single modality and rely solely on historical observations. These methods often overlook the rich semantic information and fine-grained temporal patterns. Recent studies demonstrate that additional modalities, such as text and images, are capable of providing complementary information to facilitate time series modeling [11, 46]. Specifically, the textual data often contains contextual descriptions and dataset statistics, which can enhance the understanding of time series patterns. Thus, prompt-based methods [11, 15] emerge by mapping time series into prompts to help the LLMs understand the time series in depth. These methods often focus on addressing the modality gap between continuous time series and discrete text, aiming to alleviate information misalignment [16]. However, these methods struggle to capture fine-grained temporal patterns, i.e., the ability to learn subtle dynamics, which are particularly important for ISTS forecasting to alleviate the influence of irregularity. More recent studies address this problem by converting time series into their visual versions, such as line graphs or gray-scale images, enabling spatial pattern capturing, which is

*Both authors contributed equally to this research.

[†]Corresponding author.

embedded in time series [6]. Nonetheless, these vision-based methods fall short in learning contextual semantics, since they fail to incorporate domain-specific knowledge.

As a result, we need a new kind of method that can bridge the temporal observations, textual data, and images. However, it is non-trivial to develop this kind of model, due to the following challenges. Although multimodal LLMs (MLLMs) offer a promising means to bridge this gap, leveraging their general reasoning capabilities, it is challenging to utilize MLLMs to ISTS. First, a significant representational discrepancy exists between sparse ISTS and the dense inputs required by MLLMs. Naive conversion methods, such as converting time series into standard images or plain text, may not capture the critical uneven time intervals or learn temporal patterns with missing observations. For instance, standard image resizing may distort temporal scales, while linear text serialization may lose the structural correlation across variables. Second, it is challenging to alleviate the modality gap, aligning the numerical temporal observations, text, and images. Irregular numerical observations often require high precision, whereas MLLMs operate on a coarse-grained semantic level [46]. It is urgent to invent an effective mechanism to align such threefold representations.

To address these problems, we propose *MM-ISTS*, which utilizes multimodal vision-text LLMs for ISTS forecasting. *MM-ISTS* consists of four major components: the Cross-Modal Vision-Text Encoding module, the ISTS Encoding module, the Adaptive Query-Based Feature Extractor, and the Multimodal Alignment. Specifically, *MM-ISTS* employs a Cross-Modal Vision-Text Encoding module to automatically transform ISTS to vision and text modality, which can preserve irregularity to the utmost. To better understand temporal correlations, we convert the original ISTS into 3-channel images, with channels for raw observational values, missingness masks, and time intervals, enabling the MLLMs to distinguish missing data. Further, we generate descriptive textual prompts with statistics (e.g., missing rates, variable ranges) and domain knowledge to enhance the reasoning capabilities of MLLMs. Moreover, to effectively capture temporal dynamics, we propose a customized ISTS Encoding module in parallel with the Vision-Text Encoding branch, which uses a multi-view embedding mechanism to project asynchronous observations, timestamps, and variable indices into a unified latent space. This is realized by a two-stage Transformer encoder that sequentially captures intra-series temporal dependencies and inter-series variable correlations, resulting in robust numerical representations.

To efficiently align the high-dimensional semantic space of MLLMs with temporal features, we propose an Adaptive Query-Based Feature Extractor, which employs a set of learnable queries [14] to interact with MLLMs with cross-modal alignment. This mechanism acts as an information bottleneck, compressing the vast visual-textual tokens into fixed-length representations aligned with temporal features, effectively filtering out redundant noise while reducing computational overhead during the fusion stage. Finally, a Multimodal Alignment Module is designed to fuse these three-fold multimodal representations. It includes a Modality-Aware Gating network that handles irregular data statistics (such as local sparsity levels and variance) to dynamically assign importance weights across the ISTS encoding module and cross-modal vision-text encoding module. This allows the model to leverage general knowledge

from MLLMs when numerical data is missing or sparse, enabling accurate predictions with low-quality data.

Our main contributions are summarized as follows:

- To the best of our knowledge, we propose *MM-ISTS*, the first multimodal ISTS forecasting framework augmented by vision-text LLMs.
- We design a novel cross-modal vision-text encoding module that automatically converts ISTS into irregularity-aware images and prompt-enhanced text, with ISTS encoding extracting enriched temporal features.
- An innovative adaptive query-based feature extractor is proposed to compress MLLM knowledge, including a modality-aware gating mechanism, which aligns heterogeneous multimodal features, mitigating the modality gap.
- We report on experiments using real data, which offer evidence of the effectiveness of the proposals, showing that *MM-ISTS* outperforms state-of-the-art baselines.

2 Related Work

2.1 Multi-modal Time Series Forecasting

Recent studies have incorporated textual information [17] for regular time series forecasting to enhance predictive performance beyond numerical signals. For example, *Time-LLM* [11] proposes a reprogramming framework that adapts large language models for general time series forecasting. It aligns time series and textual modalities by converting time series into text prototypes and introducing a Prompt-as-Prefix mechanism to guide the LLM in transforming time series patches for prediction. *TimeCMA* [16] proposes a cross-modality alignment framework that aligns disentangled time-series embeddings with robust prompt-based embeddings from large language models. *TimeKD* [15] introduces a cross-modal LLM-based framework for multivariate time series forecasting via privileged knowledge distillation. It uses a calibrated LLM teacher with privileged information to distill the learned knowledgeable representations into a lightweight student model. Beyond text and time series modalities, *Time-VLM* [46] integrates extra vision modality by encoding time series as images and fusing the images, text, and time series with a vision-language model to enhance time series forecasting. Despite recent progress, multimodal large-model approaches are still primarily designed for regularly sampled time series (RSTS), while effective multimodal modeling for ISTS forecasting remains to be explored.

2.2 ISTS Forecasting

Existing ISTS forecasting methods [18, 20, 26, 30, 42] can be categorized into three categories. The first category focuses on modeling continuous temporal dynamics. *Latent ODE* [24] introduces continuous-time hidden state evolution via neural ordinary differential equations, while *CRU* [26] adopts a state-space formulation with Kalman filtering. The second category represents ISTS using relational or patch-based structures. *GraFITi* [37] formulates ISTS as a bipartite graph between variables and timestamps, *T-PatchGNN* [42] segments ISTS into temporal patches and models dependencies via Transformers and GNNs, and *HyperIMTS* [13] models ISTS with hypergraph structures. More recently, pre-trained

large language models (LLMs) have been explored for ISTS forecasting. ISTS-PLM [41] investigates how representation schemes affect LLMs’ ability to model ISTS, and Time-IMM [4] introduces a benchmark focusing on realistic irregular sampling. Despite these advances, most existing approaches either concentrate on unimodal ISTS or lack global contextual information to adequately model complex and dynamic data patterns.

3 Preliminary

3.1 ISTS Definition

We consider an irregularly-sampled time series (ISTS) consisting of N variables. For the n -th variable, its historical observations are denoted as $o_n = \{(t_i^n, x_i^n)\}_{i=1}^{L_n}$, where $t_i^n \in \mathbb{R}$ denotes the timestamp of the i -th observation and $x_i^n \in \mathbb{R}$ denotes the corresponding recorded value. The number of observations L_n may vary across variables, and the complete ISTS is denoted by $\mathcal{O} = \{o_n\}_{n=1}^N$.

3.2 Canonical Representation

In practice, a commonly adopted preprocessing strategy is the canonical pre-alignment representation [1, 2, 5, 24, 26, 27, 40, 43], which transforms the ISTS data \mathcal{O} into a triplet $(\mathcal{T}, \mathcal{X}, \mathcal{M})$. Here, $\mathcal{T} = [t_i]_{i=1}^L \in \mathbb{R}^L$ denotes the ordered set of unique timestamps obtained by merging all observation times across variables, i.e., $\mathcal{T} = \bigcup_{n=1}^N \{t_i^n\}_{i=1}^{L_n}$. The value matrix $\mathcal{X} = [[x_i^n]_{n=1}^N]_{i=1}^L \in \mathbb{R}^{L \times N}$ aligns multivariate observations on the unified timeline, where x_i^n records the observed value of the n -th variable at timestamp t_i if available, and is filled with zero otherwise. To explicitly distinguish real observations from filled values, a binary mask $\mathcal{M} = [[m_i^n]_{n=1}^N]_{i=1}^L \in \{0, 1\}^{L \times N}$ is introduced, where $m_i^n = 1$ indicates that variable n is observed at time t_i , and $m_i^n = 0$ otherwise. Together, the triplet $(\mathcal{T}, \mathcal{X}, \mathcal{M})$ provides a fixed-shape representation on a shared temporal grid while preserving the original irregular sampling pattern through the observation mask. To better preserve the native irregular sampling characteristics of each variable, we refer to the representation strategy in ISTS-PLM [41] and adopt a variable-independent sequence representation for ISTS. Specifically, we do not merge timestamps across variables; instead, each variable maintains its own ordered timestamps, denoted as $\mathcal{T}_n = [t_i^n]_{i=1}^{L_n} \in \mathbb{R}^{L_n}$ for the n -th variable, where L_n is the number of observations of the n -th variable and t_i^n represents the i -th observation timestamp of the n -th variable.

3.3 Irregularly-Sampled Time Series Forecasting

Given an ISTS \mathcal{O} , we define forecasting queries to specify which future values are to be predicted. For the n -th variable, a forecasting query is defined by a future timestamp q_j^n satisfying $q_j^n > \max_i t_i^n$, where $j = 1, \dots, Q_n$ denotes the query timestamps for variable n . The set of forecasting queries is denoted as $\mathcal{Q} = \{\{q_j^n\}_{j=1}^{Q_n}\}_{n=1}^N$.

The goal of ISTS forecasting is to learn a model F_θ , parameterized by θ , that maps historical observations and forecasting queries to future value predictions.

$$F_\theta(\mathcal{O}, \mathcal{Q}) \longrightarrow \hat{\mathcal{X}} = \{\{\hat{x}_j^n\}_{j=1}^{Q_n}\}_{n=1}^N, \quad (1)$$

where \hat{x}_j^n denotes the predicted value of the n -th variable at the j -th query timestamp q_j^n .

4 Methodology

We present *MM-ISTS*, a multimodal framework designed to tackle the challenges of ISTS forecasting. The core idea of MM-ISTS is to combine the precise numerical patterns learned from historical data with the general knowledge provided by pre-trained MLLMs. As illustrated in Figure 1, the framework comprises four components: (1) Cross-Modal Vision-Text Encoding module that transforms ISTS into irregularity-aware visual and textual representations; (2) Dual-stage ISTS Encoding branch that sequentially models intra-series temporal dynamics and inter-series variable correlations; (3) Adaptive Query-Based Feature Extractor that compresses high-dimensional MLLM tokens into compact, variable-aligned queries; and (4) a Multimodal Alignment module equipped with a Modality-Aware Gating mechanism for adaptive fusion.

4.1 Cross-Modal Vision-Text Encoding

To leverage the powerful reasoning capabilities of frozen MLLMs, we propose a cross-modal transformation mechanism that maps the sparse ISTS into the dense contextual spaces of vision and language, while carefully preserving critical irregularity patterns that are essential for forecasting.

4.1.1 Irregularity-Aware Image Construction. Standard time series visualization methods, such as line plots or heatmaps, often discard fine-grained temporal dynamics and introduce noise. To address this issue, we introduce a tensor-based image construction scheme that encodes observation values, missingness patterns, and temporal intervals into separate image channels.

Given an ISTS sample with N variables and maximum sequence length L , we construct a three-channel image $\mathcal{I} \in \mathbb{R}^{3 \times N \times L}$, where the height $H = N$ corresponds to variables and the width $W = L$ corresponds to the temporal axis. Since different variables in ISTS may be observed at different time points, we represent the timestamps, values, and masks independently for each variable. Each channel captures a distinct aspect:

Observed Data channel records values: $\mathbf{C}_0 \in \mathbb{R}^{N \times L}$, where each row corresponds to a variable and each column corresponds to a timestep. The pixel intensity reflects the time series value.

Missingness Mask channel encodes the sparsity pattern: $\mathbf{C}_1 \in \mathbb{R}^{N \times L}$. A pixel value of 1 indicates that the corresponding variable was observed at that time step, while 0 indicates a missing entry.

Temporal Interval channel encodes the irregularity of sampling intervals. Since different variables may be observed at different time points, we compute the time gap independently for each variable. Specifically, for variable n at time step l , we compute $\delta_l^n = t_l^n - t_{l-1}^n$, with $\delta_1^n = 0$ for the first observation. We construct $\mathbf{C}_2 \in \mathbb{R}^{N \times L}$ where $(\mathbf{C}_2)_{n,l} = \delta_l^n$.

The final irregularity-aware image \mathcal{I} is obtained by stacking these three channels:

$$\mathcal{I} = \text{Stack}(\mathbf{C}_0, \mathbf{C}_1, \mathbf{C}_2) \in \mathbb{R}^{3 \times N \times L}. \quad (2)$$

Before feeding into the MLLM, the image is resized to match the expected input resolution and normalized to the appropriate pixel value range.

4.1.2 Statistical-dominant Text Prompting. While the constructed image provides a visual representation of the ISTS, MLLMs also benefit

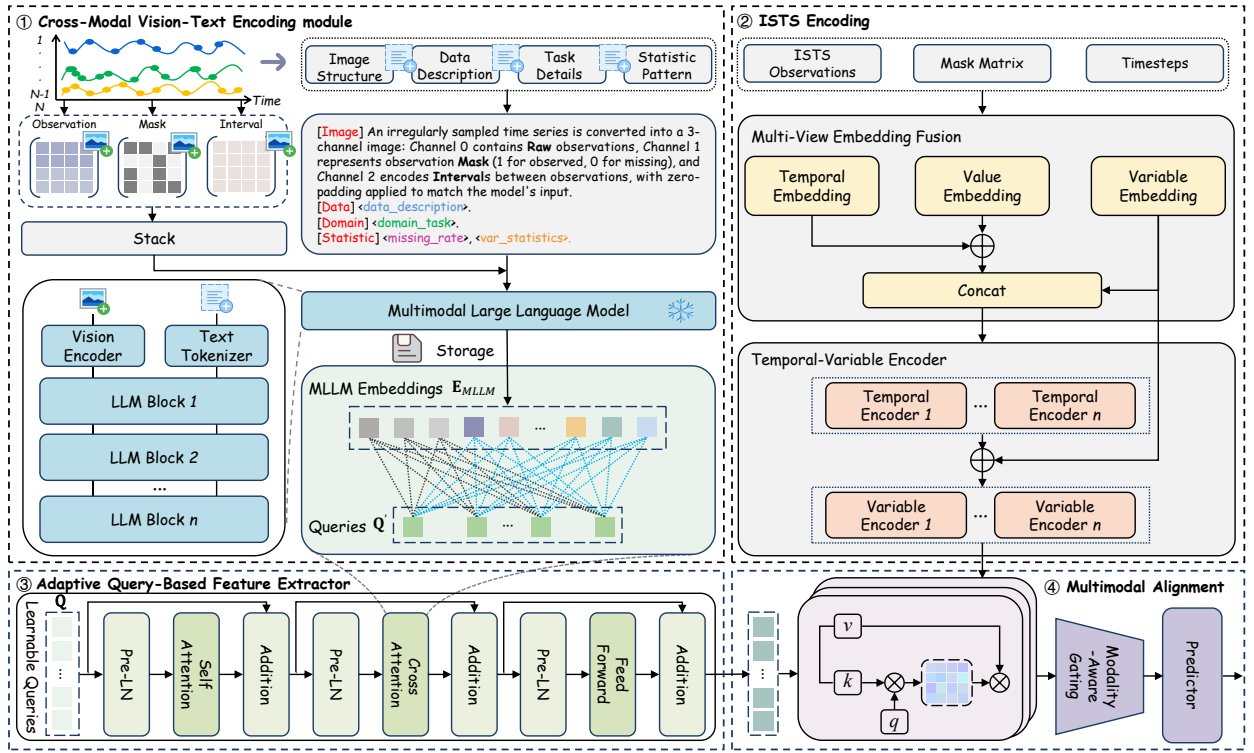


Figure 1: Overview of the proposed MM-ISTS framework.

from the textual context that activates their domain knowledge. We therefore construct a structured text prompt \mathcal{P} that integrates statistical summaries of the data with explicit domain context and task descriptions.

We first compute key summary statistics for each variable $n \in \{1, \dots, N\}$. Specifically, for each variable, we calculate the mean value over observed entries as $\mu_n = \frac{\sum_{l=1}^L m_l^n x_l^n}{\sum_{l=1}^L m_l^n}$, the value range $[x_n^{\min}, x_n^{\max}]$ where $x_n^{\min} = \min_{l:m_l^n=1} x_l^n$ and $x_n^{\max} = \max_{l:m_l^n=1} x_l^n$, and the missing rate $\rho_n = 1 - \frac{1}{L} \sum_{l=1}^L m_l^n$ representing the proportion of missing observations. To mitigate noise from extremely sparse variables where statistics are unreliable, we apply a filtering mechanism: we format the statistics into a natural language description $\mathcal{S}_n = \text{Format}(\mu_n, x_n^{\min}, x_n^{\max})$ only if $\rho_n \leq \tau$, where τ is a sparsity threshold (e.g., $\tau = 0.9$); otherwise, $\mathcal{S}_n = \emptyset$.

The final text prompt \mathcal{P} is assembled by concatenating four types of instruction components:

$$\mathcal{P} = [\mathcal{P}_{img}, \mathcal{P}_{data}, \mathcal{P}_{task}, \{\mathcal{S}_n\}_{n:\rho_n \leq \tau}], \quad (3)$$

where \mathcal{P}_{img} provides instructions for interpreting the three-channel image, \mathcal{P}_{data} supplies domain-specific context about the dataset, and \mathcal{P}_{task} specifies the forecasting objective.

4.1.3 MLLM Feature Extraction. The frozen MLLM encoder \mathcal{E}_{MLLM} jointly processes the irregularity-aware image \mathcal{I} and the structured text prompt \mathcal{P} to produce a sequence of high-dimensional hidden states. The image is first processed by a vision encoder to obtain visual tokens, which are then combined with text tokens and fed through the language model backbone.

We extract the hidden states from the deep layers of the MLLM as our multimodal representation, as these layers capture informative, rich features after cross-modal fusion:

$$\mathcal{E}_{MLLM} = \mathcal{E}_{MLLM}(\mathcal{I}, \mathcal{P}) \in \mathbb{R}^{S \times d_m}, \quad (4)$$

where S is the number of tokens output by MLLM and d_m is the hidden dimension of the MLLM. The MLLM parameters remain frozen during training, which preserves the pre-trained knowledge. Following TimeCMA [16], we pre-compute and store the MLLM token embeddings before training to improve computational efficiency.

4.2 ISTS Encoding

While MLLMs excel at high-level contextual reasoning, they may not capture fine-grained numerical patterns as accurately as dedicated time series models. Our ISTS encoder addresses this limitation by operating on carefully designed embeddings followed by a Transformer encoder that models temporal dynamics within each variable and correlations across variables.

4.2.1 Multi-View Embedding Fusion. In order to better capture the relationships within ISTS using Transformer architectures, we model them from different perspectives.

Temporal Embedding. Unlike discrete positional encodings used in standard Transformers, ISTS requires embeddings that can handle continuous and irregularly spaced timestamps. We employ a learnable sinusoidal mapping $\phi: \mathbb{R} \rightarrow \mathbb{R}^D$ that captures both periodic patterns and linear temporal trends:

$$\phi(t)_d = \begin{cases} \omega_0 t + \beta_0, & d = 0, \\ \sin(\omega_d t + \beta_d), & d > 0, \end{cases} \quad (5)$$

where $\{\omega_d\}_{d=0}^{D-1}$ and $\{\beta_d\}_{d=0}^{D-1}$ are learnable parameters. The first dimension captures linear time progression, while the remaining dimensions encode periodic patterns at different frequencies.

Variable Embedding. To distinguish between different variables and enable the model to learn variable-specific patterns, we introduce a learnable embedding matrix $\mathbf{E}_{var} \in \mathbb{R}^{N \times D}$ that assigns a unique representation $\mathbf{e}_n^{var} \in \mathbb{R}^D$ to each variable index $n \in \{1, \dots, N\}$. These embeddings are learned during training and capture the intrinsic characteristics of each variable type.

Value Embedding. For each observation, we need to encode both the numerical value and whether it was actually observed. We concatenate the observed value x_l^n with its corresponding mask indicator m_l^n and apply a linear projection: $\mathbf{e}_{l,n}^{val} = [x_l^n, m_l^n] \mathbf{W}_{val} + \mathbf{b}_{val}$, where $\mathbf{W}_{val} \in \mathbb{R}^{2 \times D}$ and $\mathbf{b}_{val} \in \mathbb{R}^D$ are learnable parameters.

Embedding Fusion. The fused embedding for the l -th time step of variable n combines temporal and value information through a mask-gated mechanism: $\mathbf{z}_{l,n} = m_l^n \cdot \phi(t_l^n) + \mathbf{e}_{l,n}^{val}$. The mask-gated design ensures that temporal information is weighted by observation presence. To enable the model to aggregate information at the variable level, we prepend the variable embedding \mathbf{e}_n^{var} as a learnable prompt token to each variable’s sequence, forming $\mathbf{Z}_n = [\mathbf{e}_n^{var}, \mathbf{z}_{1,n}, \dots, \mathbf{z}_{L,n}] \in \mathbb{R}^{(L+1) \times D}$.

4.2.2 Temporal-Variable Encoder. Multivariate ISTS exhibit two types of dependencies: temporal dependencies within each variable and cross-variable dependencies. To disentangle and effectively model these two types of relationships, we employ a Temporal Encoder and a Variable Encoder using stacked Transformer layers.

Temporal Encoder. We apply a multi-layer Transformer encoder \mathcal{F}_{temp} independently to each variable’s sequence to capture temporal patterns. The encoder consists of L_t stacked layers, where each layer applies multi-head self-attention followed by a feed-forward network. The attention mechanism allows each position to attend to all other positions within the same variable’s sequence:

$$\text{Attention}(\mathbf{Q}, \mathbf{K}, \mathbf{V}) = \text{Softmax} \left(\frac{\mathbf{Q}\mathbf{K}^\top}{\sqrt{d_k}} \right) \mathbf{V}, \quad (6)$$

where $\mathbf{Q}, \mathbf{K}, \mathbf{V} \in \mathbb{R}^{(L+1) \times d_k}$ are the query, key, and value matrices obtained by linear projections, and d_k is the dimension per attention head. The multi-head attention extends this by computing h parallel attention heads and concatenating their outputs:

$$\text{MultiHead}(\mathbf{Z}) = \text{Concat}(\text{head}_1, \dots, \text{head}_h) \mathbf{W}^O, \quad (7)$$

where $\text{head}_i = \text{Attention}(\mathbf{Z}\mathbf{W}_i^Q, \mathbf{Z}\mathbf{W}_i^K, \mathbf{Z}\mathbf{W}_i^V)$ and \mathbf{W}^O is the output projection matrix.

The Temporal Encoder processes each variable’s sequence independently, producing $\mathbf{H}_n^{temp} = \mathcal{F}_{temp}(\mathbf{Z}_n) \in \mathbb{R}^{(L+1) \times D}$. Since different variables may have different numbers of observed time points, we perform mask-aware aggregation to obtain a fixed-length representation $\mathbf{h}_n \in \mathbb{R}^D$ for each variable:

$$\mathbf{h}_n = \frac{\sum_{l=0}^L \tilde{m}_l^n \cdot \mathbf{H}_{n,l}^{temp}}{\sum_{l=0}^L \tilde{m}_l^n}, \quad (8)$$

where $\tilde{m}_0^n = 1$ for variable tokens and $\tilde{m}_l^n = m_l^n$ for $l \geq 1$.

Variable Encoder. We then model the dependencies across different variables. The aggregated variable representations are

stacked to form a matrix $\mathbf{H}_{agg} = [\mathbf{h}_1, \dots, \mathbf{h}_N]^\top \in \mathbb{R}^{N \times D}$. We enhance these representations by adding the variable embeddings and apply a multi-layer Transformer encoder \mathcal{F}_{var} consisting of L_v layers to model cross-variable correlations. The Variable Encoder allows each variable’s representation to attend to and incorporate information from all other variables. The final output is $\mathbf{H}_{ISTS} = \mathcal{F}_{var}(\mathbf{H}_{agg} + \mathbf{E}_{var}) \in \mathbb{R}^{N \times D}$.

4.3 Adaptive Query-Based Feature Extractor

While the MLLM output $\mathbf{E}_{MLLM} \in \mathbb{R}^{S \times d_m}$ encodes rich contextual information from both visual and textual modalities, it cannot be directly fused with the ISTS Encoding branch output for two key challenges: (1) the sequence length S of MLLM output varies depending on the input image and prompt, making it difficult to align with the fixed N variables; (2) the hidden dimension d_m typically differs from the ISTS encoder dimension D . To bridge this representational gap, we propose an Adaptive Query-Based Feature Extractor inspired by the Q-Former architecture [14], which acts as a learnable information bottleneck that compresses and aligns the high-dimensional MLLM output into variable-aligned representations.

We introduce a set of N learnable query tokens $\mathbf{Q} \in \mathbb{R}^{N \times d_m}$, where each query is initialized to encode a latent variable-specific representation for one of the N variables. The queries interact with the MLLM output \mathbf{E}_{MLLM} through K stacked layers, each consisting of self-attention among queries, cross-attention from queries to MLLM features, and a feed-forward network.

For each layer, the computation proceeds as follows. Given input queries \mathbf{Q} , we first apply layer normalization and self-attention to enable information exchange among the N variable queries:

$$\tilde{\mathbf{Q}} = \mathbf{Q} + \text{MultiHead}_{self}(LN(\mathbf{Q})), \quad (9)$$

where MultiHead_{self} denotes multi-head self-attention with queries, keys, and values all derived from the input.

We then apply layer normalization to obtain $\mathbf{Q}' = LN(\tilde{\mathbf{Q}})$, which serves as the query input to cross-attention. The cross-attention mechanism allows each variable query to selectively attend to and extract relevant information from the MLLM’s visual and textual representations. Specifically, we compute projected queries $\mathbf{Q}_p = \mathbf{Q}' \mathbf{W}^Q$, keys $\mathbf{K}_p = \mathbf{E}_{MLLM} \mathbf{W}^K$, and values $\mathbf{V}_p = \mathbf{E}_{MLLM} \mathbf{W}^V$, where $\mathbf{W}^Q, \mathbf{W}^K, \mathbf{W}^V$ are learnable projection matrices. The cross-attention is then computed as:

$$\text{CrossAttn}(\mathbf{Q}', \mathbf{E}_{MLLM}, \mathbf{E}_{MLLM}) = \text{Softmax} \left(\frac{\mathbf{Q}_p \mathbf{K}_p^\top}{\sqrt{d_k}} \right) \mathbf{V}_p. \quad (10)$$

The cross-attended features are added back via a residual connection:

$$\hat{\mathbf{Q}} = \tilde{\mathbf{Q}} + \text{MultiHead}_{cross}(\mathbf{Q}', \mathbf{E}_{MLLM}, \mathbf{E}_{MLLM}). \quad (11)$$

Finally, a feed-forward network with layer normalization and residual connection produces $\mathbf{Q}'' = \hat{\mathbf{Q}} + \text{FFN}(LN(\hat{\mathbf{Q}}))$. The output \mathbf{Q}'' then serves as the input \mathbf{Q} for further alignment.

Through this iterative K -layer process, the query tokens progressively extract and compress relevant contextual information from the high-dimensional visual-textual context. After K layers of

refinement, the final query states constitute our multimodal representation $\mathbf{H}_{MM} = \mathbf{Q}'' \in \mathbb{R}^{N \times d_m}$, which is explicitly aligned with the N variables in terms of the first dimension.

4.4 Multimodal Alignment

To effectively integrate precise numerical patterns with contextual knowledge, we propose an alignment module that adaptively fuses $\mathbf{H}_{ISTS} \in \mathbb{R}^{N \times D}$ and $\mathbf{H}_{MM} \in \mathbb{R}^{N \times d_m}$ based on variable-specific data quality.

Cross-Attention Fusion. Direct concatenation or addition of the two representations would not account for the contextual relationships between numerical patterns and MLLM-derived features. Instead, we use cross-attention to enable the numerical features to selectively query and incorporate relevant contextual information:

$$\mathbf{H}_{fused} = \text{CrossAttn}(\mathbf{H}_{ISTS}, \mathbf{H}_{MM}, \mathbf{H}_{MM}) \in \mathbb{R}^{N \times D}, \quad (12)$$

where \mathbf{H}_{ISTS} serves as query and \mathbf{H}_{MM} servers as keys and values.

Modality-Aware Gating. Different variables in an ISTS may have different observation densities. For a densely observed variable, the numerical features from the ISTS encoder are reliable and should be paid more attention. Conversely, for a sparsely observed variable with high missing rates, the contextual information from MLLMs may provide more valuable information. To address such variable-specific differences in observation quality, we introduce a Modality-Aware Gating mechanism that adaptively balances the contributions of the two modalities for each variable.

For each variable n , we compute a statistics vector $\mathbf{s}_n \in \mathbb{R}^4$ that summarizes its data characteristics:

$$\mathbf{s}_n = [\mu_n, \sigma_n, \rho_n, c_n], \quad (13)$$

where μ_n is the mean of observed values, σ_n is the standard deviation, ρ_n is the missing rate, and $c_n = \sum_{t=1}^L m_t^n / L$ is the normalized observation count.

A gating network \mathcal{G} , implemented as a two-layer MLP with ReLU activation, maps this statistics vector to fusion weights:

$$[\alpha_n^{num}, \alpha_n^{mm}] = \text{Softmax}(\mathcal{G}(\mathbf{s}_n)) \in \mathbb{R}^2, \quad (14)$$

where $\alpha_n^{num} + \alpha_n^{mm} = 1$.

The final fused representation for each variable is computed as a statistics-conditioned weighted combination:

$$\mathbf{H}_{final}[n] = \alpha_n^{num} \cdot \mathbf{H}_{ISTS}[n] + \alpha_n^{mm} \cdot \mathbf{H}_{fused}[n]. \quad (15)$$

4.5 ISTS Predictor

Given the fused representation \mathbf{H}_{final} and forecasting queries $\mathbf{Q} = \{\{q_j^n\}_{j=1}^{Q_n}\}_{n=1}^N$, we generate predictions by conditioning variable features on target timestamps. For query q_j^n , the prediction is generated via an MLP:

$$\hat{x}_j^n = \text{MLP}([\mathbf{H}_{final}[n] \parallel q_j^n]). \quad (16)$$

The model is optimized end-to-end via MSE loss over all valid queries, with the MLLM backbone frozen:

$$\mathcal{L} = \frac{1}{\sum_{n=1}^N Q_n} \sum_{n=1}^N \sum_{j=1}^{Q_n} (\hat{x}_j^n - x_j^n)^2. \quad (17)$$

5 Experiments

5.1 Experimental Setup

5.1.1 Datasets. To comprehensively evaluate the effectiveness of the proposed method on ISTS forecasting, we conduct experiments on four widely used benchmark datasets: *PhysioNet* [28], *MIMIC* [12], *Human Activity* [31], and *USHCN* [19]. These datasets span diverse application domains, including healthcare, biomechanics, and climate science. We randomly split each dataset into training, validation, and test sets with a ratio of 6:2:2.

5.1.2 Baselines. To comprehensively evaluate the effectiveness of the proposed method, we compare it against a diverse set of representative baseline models for the time series forecasting task. These baselines can be broadly categorized into three groups: (1) *Regular Time Series Forecasting Models*: DLinear [39], TimesNet [34], PatchTST [21], Crossformer [45], Graph WaveNet [36], MTGNN [35], StemGNN [3], CrossGNN [10], and FourierGNN [38]. (2) *ISTS Classification and Imputation Models*: GRU-D [5], SeFT [9], RainDrop [43], Warpformer [40], and mTAND [27]. (3) *ISTS Forecasting Models*: Latent ODEs [24], CRU [26], Neural Flows [1], T-PatchGNN [42], KAFNet [47], and ISTS-PLM [41].

5.2 Experimental Results

5.2.1 Main Results. Table 1 presents the forecasting performance of MM-ISTS and all baseline methods across four ISTS datasets. Key findings are summarized as follows. Different types of baselines show distinct performance gaps. Methods designed for regular time series perform the worst on most datasets, as they cannot naturally model irregular sampling patterns. ISTS classification and imputation models perform better by directly handling irregular data, but their lack of optimization for forecasting tasks leads to inferior results compared to specialized ISTS forecasting methods. Among the specialized ISTS forecasting models, T-PatchGNN, KAFNet, and ISTS-PLM represent the strongest competitors, for they have components specifically designed for irregularities. Our proposed MM-ISTS achieves the best performance on most metrics and ranks second on the remaining ones, demonstrating consistent superiority across all datasets. On average, it outperforms all ISTS forecasting baselines by **14.3%** in MSE and **15.1%** in MAE. This strong and stable performance can be largely attributed to its effective method design for ISTS: a temporal-variable encoder captures temporal and cross-variable dependencies from numerical observations, while pre-trained MLLMs provide complementary multimodal information, and the multimodal alignment module effectively combines the strengths of both information sources. Compared with the LLM-based baseline ISTS-PLM, MM-ISTS yields notable improvements. Specifically, it achieves 5.2% lower MSE and 4.6% lower MAE on the MIMIC dataset, and 5.4% lower MSE with 4.1% lower MAE on the Human Activity dataset, which verifies the advantages of MLLMs over single-modal LLM-based approaches in ISTS forecasting.

5.2.2 Ablation Study. To thoroughly investigate the contribution of major components in MM-ISTS, we conduct ablation studies on PhysioNet and Human Activity datasets. We compare the full model with four variants: *w/o Text*, which removes the statistical-semantic textual modality; *w/o Image*, which excludes the irregularity-aware

Table 1: Overall performance comparison on four datasets. The best results are highlighted in bold, and the second-best are underlined.

Dataset	PhysioNet		MIMIC		Human Activity		USHCN	
Metric	MSE $\times 10^{-3}$	MAE $\times 10^{-2}$	MSE $\times 10^{-2}$	MAE $\times 10^{-2}$	MSE $\times 10^{-3}$	MAE $\times 10^{-2}$	MSE $\times 10^{-1}$	MAE $\times 10^{-1}$
DLinear	41.86 \pm 0.05	15.52 \pm 0.03	4.90 \pm 0.00	16.29 \pm 0.05	4.03 \pm 0.01	4.21 \pm 0.01	6.21 \pm 0.00	3.88 \pm 0.02
TimesNet	16.48 \pm 0.11	6.14 \pm 0.03	5.88 \pm 0.08	13.62 \pm 0.07	3.12 \pm 0.01	3.56 \pm 0.02	5.58 \pm 0.05	3.60 \pm 0.04
PatchTST	12.00 \pm 0.23	6.02 \pm 0.14	3.78 \pm 0.03	12.43 \pm 0.10	4.29 \pm 0.14	4.80 \pm 0.09	5.75 \pm 0.01	3.57 \pm 0.02
Crossformer	6.66 \pm 0.11	4.81 \pm 0.11	2.65 \pm 0.10	9.56 \pm 0.29	4.29 \pm 0.20	4.89 \pm 0.17	5.25 \pm 0.04	3.27 \pm 0.09
Graph Wavenet	6.04 \pm 0.28	4.41 \pm 0.11	2.93 \pm 0.09	10.50 \pm 0.15	2.89 \pm 0.03	3.40 \pm 0.05	5.29 \pm 0.04	3.16 \pm 0.09
MTGNN	6.26 \pm 0.18	4.46 \pm 0.07	2.71 \pm 0.23	9.55 \pm 0.65	3.03 \pm 0.03	3.53 \pm 0.03	5.39 \pm 0.05	3.34 \pm 0.02
StemGNN	6.86 \pm 0.28	4.76 \pm 0.19	1.73 \pm 0.02	7.71 \pm 0.11	8.81 \pm 0.37	6.90 \pm 0.02	5.75 \pm 0.09	3.40 \pm 0.09
CrossGNN	7.22 \pm 0.36	4.96 \pm 0.12	2.95 \pm 0.16	10.82 \pm 0.21	3.03 \pm 0.10	3.48 \pm 0.08	5.66 \pm 0.04	3.53 \pm 0.05
FourierGNN	6.84 \pm 0.35	4.65 \pm 0.12	2.55 \pm 0.03	10.22 \pm 0.08	2.99 \pm 0.02	3.42 \pm 0.02	5.82 \pm 0.06	3.62 \pm 0.07
GRU-D	5.59 \pm 0.09	4.08 \pm 0.05	1.76 \pm 0.03	7.53 \pm 0.09	2.94 \pm 0.05	3.53 \pm 0.06	5.54 \pm 0.38	3.40 \pm 0.28
SeFT	9.22 \pm 0.18	5.40 \pm 0.08	1.87 \pm 0.01	7.84 \pm 0.08	12.20 \pm 0.17	8.43 \pm 0.07	5.80 \pm 0.19	3.70 \pm 0.11
RainDrop	9.82 \pm 0.08	5.57 \pm 0.06	1.99 \pm 0.03	8.27 \pm 0.07	14.92 \pm 0.14	9.45 \pm 0.05	5.78 \pm 0.22	3.67 \pm 0.17
Warpformer	5.94 \pm 0.35	4.21 \pm 0.12	1.73 \pm 0.04	7.58 \pm 0.13	2.79 \pm 0.04	3.39 \pm 0.03	5.25 \pm 0.05	3.23 \pm 0.05
mTAND	6.23 \pm 0.24	4.51 \pm 0.17	1.85 \pm 0.06	7.73 \pm 0.13	3.22 \pm 0.07	3.81 \pm 0.07	5.33 \pm 0.05	3.26 \pm 0.10
Latent-ODE	6.05 \pm 0.57	4.23 \pm 0.26	1.89 \pm 0.19	8.11 \pm 0.52	3.34 \pm 0.11	3.94 \pm 0.12	5.62 \pm 0.03	3.60 \pm 0.12
CRU	8.56 \pm 0.26	5.16 \pm 0.09	1.97 \pm 0.02	7.93 \pm 0.19	6.97 \pm 0.78	6.30 \pm 0.47	6.09 \pm 0.17	3.54 \pm 0.18
Neural Flow	7.20 \pm 0.07	4.67 \pm 0.04	1.87 \pm 0.05	8.03 \pm 0.19	4.05 \pm 0.13	4.46 \pm 0.09	5.35 \pm 0.05	3.25 \pm 0.05
T-PatchGNN	<u>5.11 \pm 0.11</u>	<u>3.73 \pm 0.11</u>	<u>1.66 \pm 0.02</u>	<u>7.21 \pm 0.14</u>	2.79 \pm 0.11	3.24 \pm 0.07	5.03 \pm 0.04	3.14 \pm 0.09
KAFNet	<u>5.47 \pm 0.07</u>	<u>3.82 \pm 0.12</u>	<u>1.70 \pm 0.02</u>	<u>7.23 \pm 0.04</u>	2.70 \pm 0.05	<u>3.16 \pm 0.03</u>	5.19 \pm 0.14	3.17 \pm 0.10
ISTS-PLM	5.17 \pm 0.13	<u>3.67 \pm 0.06</u>	1.72 \pm 0.05	<u>7.18 \pm 0.34</u>	<u>2.61 \pm 0.07</u>	<u>3.19 \pm 0.07</u>	5.28 \pm 0.05	<u>3.03 \pm 0.06</u>
MM-ISTS (Ours)	4.98 \pm 0.11	3.54 \pm 0.05	1.63 \pm 0.02	6.85 \pm 0.07	2.47 \pm 0.01	3.06 \pm 0.02	<u>5.10 \pm 0.03</u>	2.94 \pm 0.05

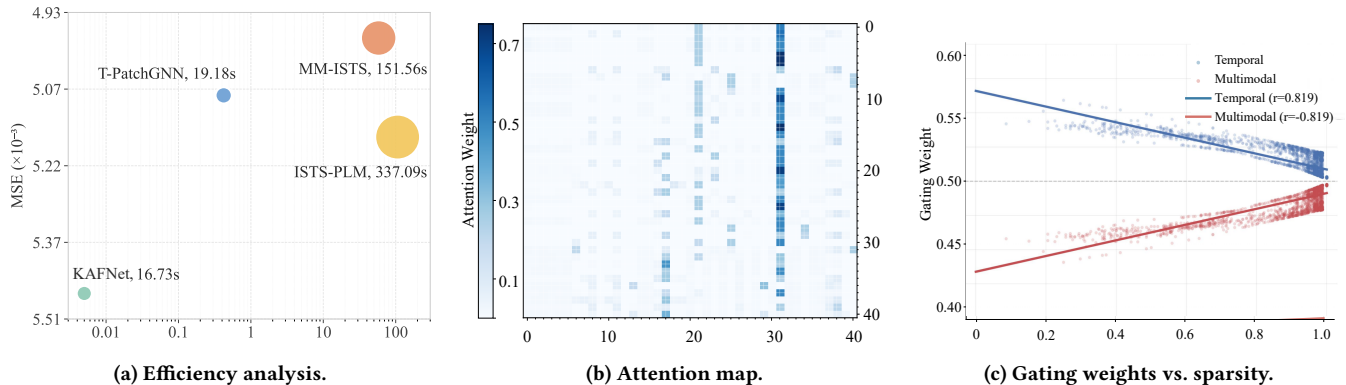
**Figure 2: (a) Efficiency comparison, (b) cross-attention patterns, and (c) adaptive gating behavior.**

image representation; *w/o QBE*, which replaces the proposed Query-Based Extractor (QBE) with simple average pooling over MLLM features; and *w/o Align*, which substitutes the multimodal alignment module with a naive element-wise addition. As illustrated in Figure 3, removing any component consistently leads to noticeable performance degradation on both datasets. Among all variants, *w/o QBE* suffers the most significant performance drop, by explicitly querying MLLM representations with variable-specific embeddings, QBE effectively compresses high-dimensional multimodal features while preserving variable-level correlations. *w/o Text* also shows a clear degradation, especially on the PhysioNet

dataset. This suggests that the statistical-semantic textual descriptions provide valuable domain-level priors that help the MLLM better capture temporal dynamics. Similarly, the performance drop observed in *w/o Image* demonstrates the importance of the proposed irregularity-aware image construction. Finally, *w/o Align* consistently underperforms the full model. The proposed multimodal alignment enables the model to adaptively balance numerical and multimodal features. In contrast, simple element-wise addition fails to model cross-modal interactions, leading to poor performance.

5.2.3 Parameter Sensitivity. We investigate the sensitivity of MM-ISTS to key hyperparameters on the PhysioNet dataset in Figure 4. We evaluate learning rates from $\{10^{-5}, 5 \times 10^{-5}, 10^{-4}, 5 \times 10^{-4}\}$. As

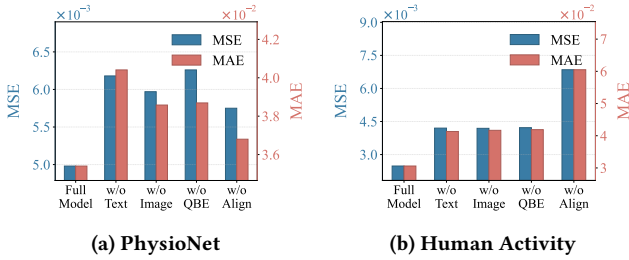


Figure 3: Ablation study.

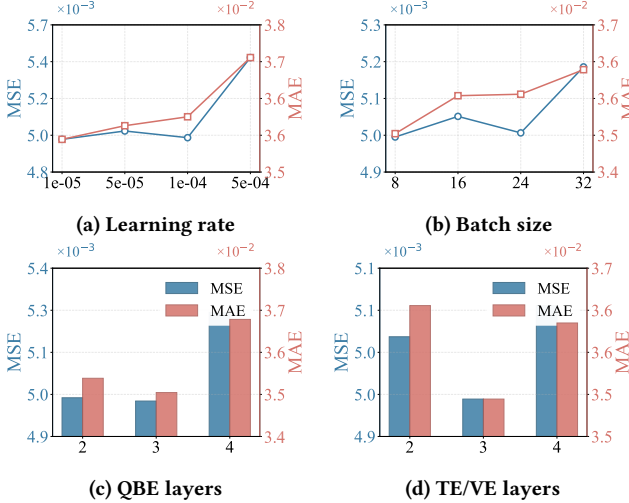


Figure 4: Hyperparameter sensitivity analysis on PhysioNet.

shown in Figure 4 (a), a learning rate of 10^{-5} yields the best performance, while larger learning rates lead to performance degradation due to unstable optimization. We test batch sizes from $\{8, 16, 24, 32\}$. Figure 4 (b) shows that smaller batch sizes achieve better performance, with batch size 8 being optimal. This benefit likely stems from the implicit regularization effect in stochastic gradient descent. We vary the number of Query-Based Extractor layers in $\{2, 3, 4\}$. As shown in Figure 4 (c), 3 layers achieve the best results, indicating that moderate depth provides sufficient capacity for feature extraction without overfitting. We also evaluate the depth of Temporal Encoder and Variable Encoder in $\{2, 3, 4\}$. Figure 4 (d) demonstrates that 3 layers yield optimal performance, balancing model expressiveness and generalization.

5.2.4 Efficiency Analysis. In Figure 2 (a), we compared the computational efficiency of MM-ISTS with two small models, such as KAFNet and T-PatchGNN, and an LLM-based model, ISTS-PLM. Since both MM-ISTS and ISTS-PLM rely on large language models, we focused on comparing their efficiencies and MSE. ISTS-PLM fine-tunes the parameters of the language model during training, while MM-ISTS fully freezes the backbone structure of the large language model and only trains the lightweight downstream modules. Therefore, the time required by MM-ISTS per cycle is approximately half of that of ISTS-PLM, and it has significantly fewer trainable parameters. Although traditional methods like KAFNet and T-PatchGNN are faster due to their smaller model size, MM-ISTS achieves significantly better prediction performance by leveraging the rich

Table 2: Effect of Different Qwen2-VL Hidden Layers.

Layer Position	MSE $\times 10^{-3}$	MAE $\times 10^{-2}$
Last	2.49 ± 0.03	3.08 ± 0.03
3rd-to-last	2.47 ± 0.01	3.06 ± 0.02
5th-to-last	2.48 ± 0.02	3.06 ± 0.02
7th-to-last	2.49 ± 0.02	3.07 ± 0.03

semantic knowledge in the frozen large language model, demonstrating a good balance between efficiency and accuracy.

5.2.5 Case Study. Figure 2 (b) visualizes the attention map in the Multimodal Alignment module, where ISTS features selectively attend to informative multimodal tokens. The sparse attention pattern indicates that the model filters noise and focuses on the most relevant information from the MLLM output. Figure 2 (c) displays the relationship between modality-aware gating weights and variable sparsity. We observe a clear trend: variables with high missing rates are assigned higher weights for the multimodal branch, while densely observed variables rely more on the numerical branch. This empirically validates our design motivation that the outputs of MLLM serve as effective complementary information when numerical data is scarce.

5.2.6 Hidden layer of MLLM. We investigate the impact of extracting hidden states from different layers of the Qwen2-VL-2B-Instruct [33]. As shown in Table 2, we evaluate four layer positions counting backward from the final layer on Human Activity [31]. The results reveal that the 3rd-to-last layer achieves the best performance with the lowest MSE and MAE, as well as the smallest variance. Interestingly, extracting features from the last layer does not yield optimal results. This phenomenon can be attributed to the fact that the last layer of MLLMs is typically optimized for next-token prediction in language generation. In contrast, the intermediate layers retain richer and more generalizable multimodal semantic representations. Furthermore, we observe that extracting from earlier layers (e.g., 7th-to-last) leads to performance degradation, likely because cross-modal fusion in transformer-based MLLMs becomes more complete in deeper layers. Notably, despite these variations, all layer configurations yield comparable results with only minor fluctuations, indicating that MM-ISTS is robust to the choice of hidden layer and that the MLLM representations are also beneficial across different depths.

6 Conclusion

We present MM-ISTS, a multimodal forecasting framework for ISTS. To overcome the representational and modality gaps inherent in ISTS, we introduce a cross-modal encoding strategy that transforms sparse ISTS into irregularity-aware visual and textual representations. By combining ISTS representations with a temporal-variable encoder and pretrained MLLMs, MM-ISTS effectively captures both numerical dynamics and complementary semantic information. Furthermore, an adaptive query-based feature extractor is adopted to efficiently compress high-dimensional MLLM tokens into compact, variable-aligned queries. Finally, Multimodal Alignment further aligns multimodal features with variable-level temporal representations with cross-attention and a modality-aware gating mechanism. Experiments on multiple real-world benchmarks demonstrate

consistent performance improvements over state-of-the-art ISTS forecasting methods and recent LLM-based baselines, highlighting the potential of multimodal learning for ISTS forecasting.

References

- [1] Marin Bilos, Johanna Sommer, Syama Sundar Rangapuram, Tim Januschowski, and Stephan Günnemann. 2021. Neural Flows: Efficient Alternative to Neural ODEs. In *NeurIPS*. 21325–21337.
- [2] Edward De Brouwer, Jaak Simm, Adam Arany, and Yves Moreau. 2019. GRU-ODE-Bayes: Continuous Modeling of Sporadically-Observed Time Series. In *NeurIPS*. 7377–7388.
- [3] Defu Cao, Yujing Wang, Juanyong Duan, Ce Zhang, Xia Zhu, Congrui Huang, Yunhai Tong, Bixiong Xu, Jing Bai, Jie Tong, and Qi Zhang. 2020. Spectral Temporal Graph Neural Network for Multivariate Time-series Forecasting. In *NeurIPS*.
- [4] Ching Chang, Jeehyun Hwang, Yidan Shi, Haixin Wang, Wen-Chih Peng, Tien-Fu Chen, and Wei Wang. 2025. Time-IMM: A Dataset and Benchmark for Irregular Multimodal Multivariate Time Series. In *NeurIPS*.
- [5] Zhengping Che, Sanjay Purushotham, Kyunghyun Cho, David Sontag, and Yan Liu. 2018. Recurrent neural networks for multivariate time series with missing values. *Scientific reports* 8, 1 (2018), 6085.
- [6] Mouxiang Chen, Lefei Shen, Zhuo Li, Xiaoyun Joy Wang, Jianling Sun, and Chenghao Liu. [n. d.]. VisionTS: Visual Masked Autoencoders Are Free-Lunch Zero-Shot Time Series Forecasters. In *ICML*.
- [7] Jicong Fan. 2022. Dynamic Nonlinear Matrix Completion for Time-Varying Data Imputation. In *AAAI*. 6587–6596.
- [8] Ary L Goldberger, Luis AN Amaral, Leon Glass, Jeffrey M Hausdorff, Plamen Ch Ivanov, Roger G Mark, Joseph E Mietus, George B Moody, Chung-Kang Peng, and H Eugene Stanley. 2000. PhysioBank, PhysioToolkit, and PhysioNet: components of a new research resource for complex physiologic signals. *circulation* 101, 23 (2000), e215–e220.
- [9] Max Horn, Michael Moor, Christian Bock, Bastian Rieck, and Karsten M. Borgwardt. 2020. Set Functions for Time Series. In *ICML*. 4353–4363.
- [10] Qihe Huang, Lei Shen, Ruixin Zhang, Shouhong Ding, Binwu Wang, Zhengyang Zhou, and Yang Wang. 2023. CrossGNN: Confronting Noisy Multivariate Time Series Via Cross Interaction Refinement. In *NeurIPS*.
- [11] Ming Jin, Shiyu Wang, Lintao Ma, Zhixuan Chu, James Y. Zhang, Xiaoming Shi, Pin-Yu Chen, Yuxuan Liang, Yuan-Fang Li, Shirui Pan, and Qingsong Wen. 2024. Time-LLM: Time Series Forecasting by Reprogramming Large Language Models. In *ICLR*.
- [12] Alistair EW Johnson, Tom J Pollard, Lu Shen, Li-wei H Lehman, Mengling Feng, Mohammad Ghassemi, Benjamin Moody, Peter Szolovits, Leo Anthony Celi, and Roger G Mark. 2016. MIMIC-III, a freely accessible critical care database. *Scientific data* 3, 1 (2016), 1–9.
- [13] Boyuan Li, Yicheng Luo, Zhen Liu, Junhao Zheng, Jianming Lv, and Qianli Ma. 2025. HyperIMTS: Hypergraph Neural Network for Irregular Multivariate Time Series Forecasting. In *ICML*.
- [14] Junnan Li, Dongxu Li, Silvio Savarese, and Steven C. H. Hoi. 2023. BLIP-2: Bootstrapping Language-Image Pre-training with Frozen Image Encoders and Large Language Models. In *ICML*, Vol. 202. 19730–19742.
- [15] Chenxi Liu, Hao Miao, Qianxiang Xu, Shaowen Zhou, Cheng Long, Yan Zhao, Ziyue Li, and Rui Zhao. 2025. Efficient Multivariate Time Series Forecasting via Calibrated Language Models with Privileged Knowledge Distillation. In *ICDE*. 3165–3178.
- [16] Chenxi Liu, Qianxiang Xu, Hao Miao, Sun Yang, Lingzheng Zhang, Cheng Long, Ziyue Li, and Rui Zhao. 2025. TimeCMA: Towards LLM-Empowered Multivariate Time Series Forecasting via Cross-Modality Alignment. In *AAAI*. 18780–18788.
- [17] Chenxi Liu, Shaowen Zhou, Qianxiang Xu, Hao Miao, Cheng Long, Ziyue Li, and Rui Zhao. 2025. Towards Cross-Modality Modeling for Time Series Analytics: A Survey in the LLM Era. In *IJCAI*. 10564–10572.
- [18] Yicheng Luo, Bowen Zhang, Zhen Liu, and Qianli Ma. 2025. Hi-Patch: Hierarchical Patch GNN for Irregular Multivariate Time Series. In *ICML*.
- [19] MJ Menne, CN Williams Jr, RS Vose, and Data Files. 2015. Long-term daily climate records from stations across the contiguous United States.
- [20] Giangiacomo Mercatali, Andre Freitas, and Jie Chen. 2024. Graph neural flows for unveiling systemic interactions among irregularly sampled time series. In *NeurIPS*. 57183–57206.
- [21] Yuqi Nie, Nam H. Nguyen, Phanwadee Sinthong, and Jayant Kalagnanam. 2023. A Time Series is Worth 64 Words: Long-term Forecasting with Transformers. In *ICLR*.
- [22] Yongkyung Oh, Dongyoung Lim, and Sungil Kim. 2024. Stable Neural Stochastic Differential Equations in Analyzing Irregular Time Series Data. In *ICLR*.
- [23] Matthew A. Reyna, Christopher Josef, Salman Seyedi, Russell Jeter, Supreeth P. Shashikumar, M. Brandon Westover, Ashish Sharma, Shamim Nemati, and Gari D. Clifford. 2019. Early Prediction of Sepsis from Clinical Data: the PhysioNet/Computing in Cardiology Challenge 2019. In *CinC*. 1–4.
- [24] Yulia Rubanova, Tian Qi Chen, and David Duvenaud. 2019. Latent Ordinary Differential Equations for Irregularly-Sampled Time Series. In *NeurIPS*. 5321–5331.
- [25] Jeffrey D Scargle. 1982. Studies in astronomical time series analysis. II-Statistical aspects of spectral analysis of unevenly spaced data. *Astrophys. J.* 263 (1982), 835–853.
- [26] Mona Schirmer, Mazin Eltayeb, Stefan Lessmann, and Maja Rudolph. 2022. Modeling Irregular Time Series with Continuous Recurrent Units. In *ICML*. 19388–19405.
- [27] Satya Narayan Shukla and Benjamin M. Marlin. 2021. Multi-Time Attention Networks for Irregularly Sampled Time Series. In *ICLR*.
- [28] Ikaro Silva, George Moody, Daniel J Scott, Leo A Celi, and Roger G Mark. 2012. Predicting in-hospital mortality of icu patients: The physionet/computing in cardiology challenge 2012. In *CinC*. 245–248.
- [29] Xianfeng Tang, Huaxiu Yao, Yiwei Sun, Charu C. Aggarwal, Prasenjit Mitra, and Suhang Wang. 2020. Joint Modeling of Local and Global Temporal Dynamics for Multivariate Time Series Forecasting with Missing Values. In *AAAI*. 5956–5963.
- [30] Yusuke Tashiro, Jiaming Song, Yang Song, and Stefano Ermon. 2021. CSDI: Conditional Score-based Diffusion Models for Probabilistic Time Series Imputation. In *NeurIPS*. 24804–24816.
- [31] Vedrana Vidulin, Mitja Lustrek, Bostjan Kaluza, Rok Piltaver, and Jana Krivec. 2010. Localization data for person activity. *UCI Machine Learning Repository* 10 (2010), C57G8X.
- [32] Roberto Vio, María Díaz-Trigo, and Paola Andreani. 2013. Irregular time series in astronomy and the use of the Lomb-Scargle periodogram. *Astron. Comput.* 1 (2013), 5–16.
- [33] Peng Wang, Shuai Bai, Sinan Tan, Shijie Wang, Zhihao Fan, Jinze Bai, Keqin Chen, Xuejing Liu, Jialin Wang, Wenbin Ge, Yang Fan, Kai Dang, Mengfei Du, Xuancheng Ren, Rui Men, Dayiheng Liu, Chang Zhou, Jingren Zhou, and Junyang Lin. 2024. Qwen2-VL: Enhancing Vision-Language Model’s Perception of the World at Any Resolution. *CoRR* abs/2409.12191 (2024).
- [34] Haixu Wu, Tengge Hu, Yong Liu, Hang Zhou, Jianmin Wang, and Mingsheng Long. 2023. TimesNet: Temporal 2D-Variation Modeling for General Time Series Analysis. In *ICLR*.
- [35] Zonghan Wu, Shirui Pan, Guodong Long, Jing Jiang, Xiaojun Chang, and Chengqi Zhang. 2020. Connecting the Dots: Multivariate Time Series Forecasting with Graph Neural Networks. In *SIGKDD*. 753–763.
- [36] Zonghan Wu, Shirui Pan, Guodong Long, Jing Jiang, and Chengqi Zhang. 2019. Graph WaveNet for Deep Spatial-Temporal Graph Modeling. In *IJCAI*. 1907–1913.
- [37] Vijaya Krishna Yalavarthi, Kiran Madhusudhanan, Randolph Scholz, Nourhan Ahmed, Johannes Burchert, Shayan Jawed, Stefan Born, and Lars Schmidt-Thieme. 2024. GraFITi: Graphs for Forecasting Irregularly Sampled Time Series. In *AAAI*. 16255–16263.
- [38] Kun Yi, Qi Zhang, Wei Fan, Hui He, Liang Hu, Pengyang Wang, Ning An, Longbing Cao, and Zhendong Niu. 2023. FourierGNN: Rethinking multivariate time series forecasting from a pure graph perspective. *NeurIPS* 36 (2023), 69638–69660.
- [39] Ailing Zeng, Muxi Chen, Lei Zhang, and Qiang Xu. 2023. Are Transformers Effective for Time Series Forecasting?. In *AAAI*. 11121–11128.
- [40] Jiawen Zhang, Shun Zheng, Wei Cao, Jiang Bian, and Jia Li. 2023. Warformer: A Multi-scale Modeling Approach for Irregular Clinical Time Series. In *SIGKDD*. 3273–3285.
- [41] Weijia Zhang, Chenlong Yin, Hao Liu, and Hui Xiong. 2025. Unleashing The Power of Pre-Trained Language Models for Irregularly Sampled Time Series. In *SIGKDD*. 3831–3842.
- [42] Weijia Zhang, Chenlong Yin, Hao Liu, Xiaofang Zhou, and Hui Xiong. 2024. Irregular Multivariate Time Series Forecasting: A Transformable Patching Graph Neural Networks Approach. In *ICML*.
- [43] Xiang Zhang, Marko Zeman, Theodoros Tsiligkaridis, and Marinka Zitnik. 2022. Graph-Guided Network for Irregularly Sampled Multivariate Time Series. In *ICLR*.
- [44] Yudong Zhang, Xu Wang, Xuan Yu, Zhengyang Zhou, Xing Xu, Lei Bai, and Yang Wang. 2025. DIFFODE: Neural ODE with Differentiable Hidden State for Irregular Time Series Analysis. In *ICDE*. 1–14.
- [45] Yunhao Zhang and Junchi Yan. 2023. Crossformer: Transformer Utilizing Cross-Dimension Dependency for Multivariate Time Series Forecasting. In *ICLR*.
- [46] Siru Zhong, Weilin Ruan, Ming Jin, Huan Li, Qingsong Wen, and Yuxuan Liang. 2025. Time-VLM: Exploring Multimodal Vision-Language Models for Augmented Time Series Forecasting. In *ICML*.
- [47] Ziyu Zhou, Yiming Huang, Yanyun Wang, Yuankai Wu, James T. Kwok, and Yuxuan Liang. 2026. Revitalizing Canonical Pre-Alignment for Irregular Multivariate Time Series Forecasting. In *AAAI*.